NASA / CR—2001-210468

# Investigation Into Spectroscopic Techniques for Thermal Barrier Coating Spall Detection

Wim de Groot
Dynacs Engineering Company, Inc., Brook Park, Ohio

Beth Opila
Cleveland State University, Cleveland, Ohio

January 2001

## The NASA STI Program Office . . . in Profile

Since its founding, NASA has been dedicated to the advancement of aeronautics and space science. The NASA Scientific and Technical Information (STI) Program Office plays a key part in helping NASA maintain this important role.

The NASA STI Program Office is operated by Langley Research Center, the Lead Center for NASA's scientific and technical information. The NASA STI Program Office provides access to the NASA STI Database, the largest collection of aeronautical and space science STI in the world. The Program Office is also NASA's institutional mechanism for disseminating the results of its research and development activities. These results are published by NASA in the NASA STI Report Series, which includes the following report types:

- TECHNICAL PUBLICATION. Reports of completed research or a major significant phase of research that present the results of NASA programs and include extensive data or theoretical analysis. Includes compilations of significant scientific and technical data and information deemed to be of continuing reference value. NASA's counterpart of peer-reviewed formal professional papers but has less stringent limitations on manuscript length and extent of graphic presentations.

- TECHNICAL MEMORANDUM. Scientific and technical findings that are preliminary or of specialized interest, e.g., quick release reports, working papers, and bibliographies that contain minimal annotation. Does not contain extensive analysis.

- CONTRACTOR REPORT. Scientific and technical findings by NASA-sponsored contractors and grantees.

- CONFERENCE PUBLICATION. Collected papers from scientific and technical conferences, symposia, seminars, or other meetings sponsored or cosponsored by NASA.

- SPECIAL PUBLICATION. Scientific, technical, or historical information from NASA programs, projects, and missions, often concerned with subjects having substantial public interest.

- TECHNICAL TRANSLATION. English-language translations of foreign scientific and technical material pertinent to NASA's mission.

Specialized services that complement the STI Program Office's diverse offerings include creating custom thesauri, building customized data bases, organizing and publishing research results . . . even providing videos.

For more information about the NASA STI Program Office, see the following:

- Access the NASA STI Program Home Page at ***http://www.sti.nasa.gov***

- E-mail your question via the Internet to help@sti.nasa.gov

- Fax your question to the NASA Access Help Desk at 301–621–0134

- Telephone the NASA Access Help Desk at 301–621–0390

- Write to:
  NASA Access Help Desk
  NASA Center for AeroSpace Information
  7121 Standard Drive
  Hanover, MD 21076

NASA / CR—2001-210468

# Investigation Into Spectroscopic Techniques for Thermal Barrier Coating Spall Detection

Wim de Groot
Dynacs Engineering Company, Inc., Brook Park, Ohio

Beth Opila
Cleveland State University, Cleveland, Ohio

Prepared under Contract NAS3–98008

National Aeronautics and
Space Administration

Glenn Research Center

January 2001

## Acknowledgments

The authors would like to acknowledge the contributions of Dr. Nathan Jacobson, Jim Gauntner, George Madzsar, and Dr. Robert Miller. This work was funded by the Glenn Research Center Director's Discretionary Fund.

This report is a formal draft or working paper, intended to solicit comments and ideas from a technical peer group.

This report contains preliminary findings, subject to revision as analysis proceeds.



Available from

NASA Center for Aerospace Information
7121 Standard Drive
Hanover, MD 21076
Price Code: A03

National Technical Information Service
5285 Port Royal Road
Springfield, VA 22100
Price Code: A03

Available electronically at http://gltrs.grc.nasa.gov/GLTRS

# Investigation Into Spectroscopic Techniques for Thermal Barrier Coating Spall Detection

Wim de Groot
Dynacs Engineering Company, Inc.
Brook Park, Ohio 44142

Beth Opila
Cleveland State University
Cleveland, Ohio 44115

## Abstract

Spectroscopic methods are proposed for detection of thermal barrier coating (TBC) spallation from engine hot zone components. These methods include absorption and emission of airborne marker species originally embedded in the TBC bond coat. In this study, candidate marker materials for this application were evaluated. Thermochemical analysis of candidate marker materials, combined with additional constraints such as toxicity and uniqueness to engine environment, provided a short list of four potential species: platinum, copper oxide, zinc oxide, and indium. The melting point of indium was considered to be too low for serious consideration. The other three candidate marker materials, platinum, copper oxide, and zinc oxide, were placed in a high temperature furnace, and emission and absorption properties were measured over a temperature range from 800 – 1400 °C and a spectral range from 250 to 18000 nm. Platinum did not provide the desired response, likely due to the low vapor pressure of the metallic species and the low absorption of the oxide species. It was also found, however, that platinum caused a broadening of the carbon dioxide absorption at 4300 nm. The nature of this effect is not known. Absorption and emission caused by sodium and potassium impurities in the platinum were found in the platinum tests. Zinc oxide did not provide the desired response, again, most likely due to the low vapor pressure of the metallic species and the low absorption of the oxide species. Copper oxide generated two strongly temperature dependent absorption peaks at 324.8 and 327.4 nm. The melting point of copper oxide was determined to be too low for serious consideration as marker material.

## Introduction

A regularly scheduled and costly maintenance item for all turbo-engine equipped planes is the inspection of the thermal barrier coatings (TBC) on turbine blades. The inspection of these coatings requires the engine to be taken out of operation and to be partly disassembled for providing access to the TBC for boroscope observation. A typical mode of operation for this maintenance is a visual inspection of the TBC for cracks, erosion or other damage that will indicate the remaining TBC life. This type of maintenance is costly because it is skilled-labor-intensive, and it requires that the engine be out of service. In order to assure safe flight conditions, however, it is imperative to have these inspections done on a regular schedule.

Substantial engine maintenance cost savings and increased engine operational safety could be obtained if methods were to be developed that could detect TBC deterioration, either in flight or during engine operation in ground tests that cover the whole range of engine operating conditions. A prime candidate for such methods is the optical monitoring of engine exhaust for anomalous gaseous species. Over the last decade, a substantial effort was expended to develop optical

methods for monitoring the presence of anomalous metallic species in the plumes of rocket engines.[1] Two of the most promising devices are a nozzle mounted optic assembly, which collects emissions from the nozzle and combustion chamber, and the Fabry-Perot interferometer, which filters emission in spectral regions that characterizes specific species radiation. Both devices were developed for in-flight health monitoring by continuously monitoring the rocket engine exhaust for specific materials that could erode during the high performance part of the flight. Demonstrations of these devices on Space Shuttle Main Engine (SSME) test runs[1] showed substantial emissions of chromium (Cr), nickel (Ni), and iron (Fe), all originating from stainless steel components inside the engine. A detailed list of these stainless components and their alloy constituents is provided by Paradis.[2] Typical spectra with and without metallic contaminants are shown in Figure 1.

Similar metallic spectra were obtained during in-house materials-combustion compatibility tests for satellite propulsion systems.[3] Stainless steel samples were placed inside a small hydrogen-oxygen combustor at an O/F mixture ratio of 4, at 3 bar pressure, and above 2000 K temperature. A spectroscopic system collected emission from the flow behind the reacting solid stainless steel. The acquired spectra showed strong emission features at three different spectral wavelengths, as shown in Figure 2. The strongest emission lines were identified to be chromium (Fig. 2.a) and some of the weaker lines were identified to be nickel (Fig. 2.b). The detection of iron was slightly more difficult due to the fact that a strong iron emission line is located in between hydroxyl radical emission lines, whereas the nickel lines lie below and the chromium lines lie above the dominant OH spectral bands. In order to find the iron line, therefore, the emission spectra without (lower) and with (upper) installed stainless sample should be compared, as is shown in Fig. 2.c.

An ideal engine monitoring system would correctly identify the engine part before it fails. The three metals detected in the above two examples, however, show up in virtually all engine components and therefore, if present in the exhaust gas, would not be good marker materials for identifying which engine component exhibits wear. They could, however, indicate problem spots in other engine components, and should therefore be monitored in the exhaust. Due to the extreme environment it experiences, one engine sub-component most often associated with failure is the TBC on the turbine blades. For that reason, the current project is focused on identifying a “marker” species that can, without adverse effect, be embedded inside the TBC bond coat. When detected in the exhaust, that marker would specifically point to TBC spallation or failure. A possible marker could be platinum, already found in the TBC bond coat of one engine manufacturer.

The examples provided thus far all focused on emission, which is the simplest optical monitoring method, due to the fact that no separate light source is required. Depending on the marker species, however, optical absorption is an alternate candidate around which a wear-or-failure monitoring system could be developed. The equipment used to monitor emission and/or absorption typically consists of a monochromator to separate the emission wavelengths and a detector. Additionally, a light source is required for absorption. Low cost equipment for both techniques can be purchased and integrated with fiber-optics for in-flight monitoring of TBC health. Absorption would be appropriate when the gas temperature is moderately low and gas molecules would populate lower energetic levels where up-transitions with the help of energy quanta from an external source could be accomplished. Such conditions exist in the exhaust of the gas turbine engine.

Following the identification of marker species and the possible adjustments of TBC bond coatings to accommodate these marker species, an effort to develop instrumentation to facilitate their detection has been projected. A two-track development process is envisioned. Initially, the instrumentation would be designed inside a package, which could be wheeled to the back of a

mounted airplane engine. While idling, the exhaust could be checked. In order to assure a higher degree of safety, the same check could be done with the engine at full throttle. To incorporate such health checking does have the potential to extend the intervals between intrusive engine checks and maintenance. A more ambitious part of the instrumentation development would be to miniaturize all equipment and to utilize optical fibers for mounting an in-flight monitoring package for hot section health monitoring. Such miniaturization development, currently feasible, would be a substantial addition to the overall safety monitoring of engines during flight. Other spectroscopic monitoring techniques have been identified,[2] but no critical breakthrough in accomplishing in-flight TBC health monitoring has been made thus far.

The goal of this project was to identify a material compatible with the TBC bond coat that would be detectable by a spectroscopic technique. As the TBC cracked or spalled from the underlying bond coat alloy, volatile species of this marker material would form in the combustion environment and be detected by the spectroscopic technique. The approach of this project was to identify potential marker materials using a thermochemical screening process, spectroscopically detect these species in a simulated combustion environment in a furnace, and finally demonstrate the utility of this technique using TBC coated specimens in a burner rig. This paper addresses the first two aspects of the project, namely, thermochemical screening and furnace tests of candidate marker materials.

Theory

Metal species in flames appear as atomic-, metal oxide-, or metal hydroxide- vapor, depending on the chemical environment created by the fuel/oxidizer. Each of those species can be excited by any means such as flames, shocks, arcs, sparks, etc. to internal energy levels which are not stable under the Boltzmann chemical equilibrium. The internal energy picked up from the excitation mechanism will appear as electronic excitation in atomic species, or as internal vibrational- and/or rotational excitation in the oxides and hydroxides. The species equilibrate (jump energy level while exchanging or releasing energy) with their environment by collisional equilibration (quenching) and/or emission/absorption of radiation. Typically, transitions between electronic energy levels involve larger energy quantas as compared to transitions between vibrational and rotational energy level. When atomic species (electronic energy levels only) equilibrate, the energy quanta are substantial and the emission released during the transition, therefore, corresponds to emitted energy in the ultraviolet (UV), or low visible range of the spectrum. Molecular species typically equilibrate while emitting near- to mid-infrared (IR), as the result of the small difference in internal vibrational/rotational energy levels.

Ignoring collisional energy redistribution, the intensity of emitted light, I, for the above described transitions can be given by:

$$I = \frac{A_{ij} N_k h\nu g_i e^{(-E_i/kT)}}{Z(T)} \tag{1}$$

where $A_{ij}$ is the transition probability between the initial and final internal energy state, $N_k$ is the number density of species k, $h\nu$ is the photon energy (h is Planck's constant, $\nu$ is the photon wavelength) , $g_i$ is the statistical weight, $E_i$ is the energy level of the initial state, $k$ is Boltzmann's constant, $T$ is the gas dynamic temperature, and $Z(T)$ is the species partition function. Without going into much detail, it can be seen that the intensity varies linearly with $N_k$ and $A_{ij}$ , and has a complex relationship with T. In order to use the emitted light as a good indicator of species presence, it is important to have a substantial transition probability such that even minute species

presence will generate a detectable emission. The expanding flow in the high temperature engine environment generates species emission proportional to the local equilibrium species number density residing at the upper energy level of the transition. During the expansion, thermal energy is converted into kinetic energy of motion. The flow temperature drops, and all flow species equilibrate, either by collisional mechanisms or by radiating energy, thus emission.

The examples given in Figures 1 and 2 all focused on emission, which is the simplest optical monitoring technique, due to the fact that no radiation source is required. Depending on the marker species, however, upper energy levels are frequently not highly populated at the temperatures under consideration, and no detectable emission will occur. In order to have substantial detection sensitivity at lower temperatures, emission monitoring is frequently exchanged for absorption monitoring. In this approach, a light source (laser, broadband lamp) is used to illuminate the flow. The transmitted intensity at a wavelength that corresponds to the up-transition is monitored. A reduced intensity indicates light absorption and the presence of the species under evaluation. Depending on the molecular species and the quantum jump of the transition, such absorption spectra can appear as single absorption lines, absorption bands, or series of absorption bands. An example of the latter absorption spectrum is given in Figure 3, where a heated iodine cell containing crystallized $I_2$ in vacuum provides a pure iodine vapor, well characterized by Forkey et al.[4]

## Material Selection

### Selection of Candidate Marker Materials

The desired properties of a marker material include:

1. Unique to the hot section environment. The following elements were rejected as candidate materials since they are common in the hot section environment: Fe, Cr, Ni, Y, Zr. In addition the impurities Na and K were rejected as marker materials due to their ubiquitous presence in the environment.
2. Non-toxic materials. Be and Cd were rejected due to their toxicity.

The remaining materials were subjected to a thermochemical property screen as discussed below to determine if the following criteria were met.

3. Detectable vapor pressure. Materials with a vapor pressure greater than $10^{-10}$ atm at 1400K were selected for further evaluation.
4. The vapor pressure of the volatile species should have a strong temperature dependence so that as the TBC fails and a hot spot develops, a definitive increase in the partial pressure of the volatile species is observed.
5. High melting point of marker material.

Attempts were made to locate the thermochemical data of each element in the periodic table (as well as the solid oxides of each element) and their corresponding atomic, oxide and hydroxide vapor species. Sources of thermochemical data included JANAF,[5] SGTE,[6] IVTANTHERMO,[7] Glushko,[8] Krikorian,[9] Ebbinghaus,[10] and Hashimoto.[11] The data were input into the chemical equilibrium free energy minimization package, ChemSage.[12] The phase equilibrium between the solid candidate marker material and the fuel-lean combustion environment, equivalence ratio of 0.5, (6.7% $CO_2$, 7.8% $H_2O$, 10.6% $O_2$, 74.9% $N_2$) was examined. The partial pressure of all volatile species in these equilibria were determined between 1000 and 2000 °C. A summary of this screening can be found in Table I. Three materials were identified by this thermochemical

screening process to fit the criteria one through four above: CuO, ZnO, and In. Indium sublimes at 850 °C and was thus eliminated from consideration. In addition, Pt was considered since it is already present in one turbine engine manufacturer TBC system, as a platinum aluminide bond coat. The vapor pressure of volatile species of Pt, CuO, and ZnO as a function of temperature in combustion environments can be found in Figures 4a through 4c. In addition, the melting points of candidate marker materials are provided in Table II.

Spectroscopic data from the three candidate marker materials, Pt, CuO, and ZnO, identified in the first analysis as having potential applicability, are summarized in Table III. Limited information is available on spectroscopic quantities. Indeed, although thermo-chemical data indicate that the dominant oxide of platinum is platinum dioxide, only spectroscopic data of the platinum monoxide can be found in the literature.[13] The relative intensities of the atomic vapor species spectral lines are given on a different relative scale than the relative intensities of the molecular species and should not be compared with the latter. The table is more intended to provide a taste of the variety of species that could appear in the gas phase rather than to provide a quantitative data base. Spectroscopic data were collected from Pearse[13] and Brode.[14]

## Experimental

### Furnace:

The furnace setup consisted of a 99.8% pure alumina tube, 3 inch outer diameter by 36 inch length held horizontally within a 20 inches long, rectangular, high temperature furnace. The furnace hot zone was found to be within 5 °C of the desired temperature in the center two inches of the tube and within 15 °C in the center four inches. The set temperature was determined by calibration with a type R thermocouple. The thermocouple was removed from the furnace during experiments to ensure an optical line of sight through the furnace tube. Powdered samples of each candidate marker material were placed in 99.8% purity alumina boats which were 2.75" in length and centered in the hot zone of the furnace for spectroscopic detection of volatile species. The gas environment consisted of a simulated combustion environment, 79% $N_2$, 9.75% $CO_2$, 4.5% $H_2O$, and 6.75 % $O_2$. The gas flow rate was controlled using a Tylan mass flow controller with the gas velocity typically about 0.1 cm/s. Water was fed, using a peristaltic pump into a borosilicate glass capillary feedthrough in the furnace tube endcap. The water dripped into a fused quartz wool plug in the inlet side of the furnace tube at a point where the temperature was about 200 °C. Care was taken to keep the fused quartz wool out of the optical path through the furnace tube.

### Optical Setup:

Because of the variety of atomic and molecular vapor species involved, the equipment has been designed to cover the widest possible emission/absorption wavelength range that the simple experimental configuration allows, while providing the highest detection sensitivity and resolution. Table III indicates that the range of interest for atomic and monoxide species is from the mid-UV to the visible, and near infrared. The range of interest for (mostly) absorption of polyatomic species vapor is in the near-, and mid-IR range. In order to cover the full range of wavelengths, two spectroscopic configurations have been designed around the high temperature furnace, which are able to monitor the range from 250 to 1500 nm, and 2000 to 18000 nm. The range from 1500 nm to 2000 nm was not accessible with the available equipment. Absorption or emission was not expected in this range. Temperatures are varied from 800 °C through 1400 °C, with most tests done at 1200 °C.

*UV/Visible:*
The coverage of the ultraviolet and visible part of the spectrum is accomplished by the system shown in Figure 5. The two endcaps of the ceramic furnace tube are equipped with 0.5" diameter fused silica windows, transparent over the range of 250 nm to 1500 nm. An optical calibration source illuminates one endcap. The light traverses the alumina furnace tube, exits from the opposite endcap window, is collected by an optical lens and focused with the same lens onto the entrance of a 0.5 meter monochromator. The lens is selected to have a matching F# with the spectrometer. For the current hardware a F# of 4 was used. The monochromator separates the incoming light by wavelength through a refraction grating. Three gratings are used for the UV-visible part of the spectrum, all three with 1200 groove/mm grating, but optimized for 250 nm, 330 nm and 500 nm. The 1200 groove/mm grating provides a dispersion of 1.6 nm/mm and a resolution of 0.02 nm. Exchanging between these gratings assures maximum light throughput, and thus sensitivity across the full wavelength range. Test measurements with a mercury calibration lamp showed for example that the 330 nm grating provided 60% higher light throughput at 300 nm than the 500 nm grating.

A backlit, 1024 element, dual diode array is mounted on the exit plane of the monochromator, making it a spectrometer. Pixel elements are 22.4 μm wide, creating a system resolution of 0.45 nm per pixel. The dual diode array is extremely sensitive over the wavelength range analyzed. The sensitivity, however, peaks at 620 nm and drops down substantially in the mid-UV and near-IR. The wavelength range of the spectrometer can be selected by turning the grating of the monochromator remotely from the computer console, or by physically interchanging the grating. Each time the grating is changed, a wavelength calibration is required.

Computer software reads out the dual diode array intensity, and displays the spectra on the computer screen. With the described hardware, each spectrum covers approximately 40 nm spectral range. During data acquisition, spectra are obtained with 35 nm intervals, which provides overlap of 5 nm at the spectral edges to assure continuity. The software used for data acquisition and processing is the Princeton Instruments WINSPEC software.[15] The experimental arrangement described here allows for both emission and absorption of species to be detected and monitored.

*IR:*
In order to cover the mid-IR range of the spectrum, the calibration lamp, which only covers from 250 through 1500 nm is replaced with a 60 W infrared tungsten emitter. The optical windows in the endplates of the ceramic tube and the collection and focusing lens have been replaced with zinc selenide optics, which transmit radiation from 1000 through 18000 nm. The monochromator gratings for the IR range have been selected with 1200 groove/mm but optimized for 5000 nm and 12000 nm. The infrared region has been divided into two sections, which are evaluated separately. The low range of the mid-IR covers from 2000 through 8000 nm, and the high range of the mid-IR covers from 7000 to 18000 nm. A small overlap assures that phenomena, which could escape detection near the edge regions will be covered twice. The detector element is a Mercury-Cadmium-Telluride Photodetector with a sensitivity spanning the range from 2000 through 18000 nm. The fully modified system is schematically shown in Figure 6.

A photodetector is only able to measure the intensity of the light which it detects. No spectral information can be provided. In order to include the detected light as a function of wavelength, the monochromator grating moves, changing the wavelength of the light falling on the detector, in other words, the spectrum is scanned. Scanning speed and readout speed determine the sensitivity of the spectral intensity measurements. The beginning and end of each scan can be programmed into the software, as well as the scanning speed and the number of scans.

Because high temperature components always emit substantial radiation in the infrared range, the possibility exists that a possible signal is not detected due to the large background emission. In order to extract weak signals from large background noise, a lock-in detection scheme is used which modulates the source emitter, and filters the detected emission at the modulation frequency. For maximum sensitivity, digital signal processing (DSP) is used for the extraction of weak absorption. A frequency controlled "chopper wheel" modulates the frequency of the emitter, typically in the 200 to 400 Hz range. This frequency is also the reference frequency by which a lock-in amplifier separates the modulated signal from the background radiation. GRAMS[16] software from Galactic Industries allows control over the scanning functions of the monochromator as well as the photodetector intensity measurement by the lock-in amplifier/computer combination. The resulting intensity distribution is displayed on the computer screen and stored in memory. Because only the source can be modulated, maximum sensitivity can only be achieved in the absorption mode. Emission detection is feasible only if the signal to noise ratio of the unmodulated emitted radiation is sufficient.

*Experimental procedure:*
For each of the spectra observed, a number of precautions have to be taken in order to assure that the detected spectral features can be attributed to a single cause. This requires the elimination of contributions a) of carrier gas species to high temperature emission and/or absorption, b) of infrared emission by the high temperature ceramic furnace tube, and c) of the optical path outside the furnace. Each spectra is initiated by acquiring a spectrum with the furnace filled with argon gas at ambient conditions and at elevated temperature. If present, these spectra will highlight emission from the furnace walls, predominately expected in the infrared spectral range. Subsequently, spectra of the furnace filled with simulated combustion products will be acquired at ambient conditions and at elevated temperatures. For both the argon and combustion species spectra, the gas is continuously replenished. The sequence of measurements is shown in the following procedure:

1 : Collect light from broadband lamp without furnace operation
2 : Collect light from broadband lamp with furnace operation in air
3 : Collect light from broadband lamp with furnace operation in argon
4 : Collect light from broadband lamp with furnace operation and combustion gases flowing - no water
5 : Collect light from broadband lamp with furnace operation, combustion gases and water, with subtraction of spectra collected in step 3.
6 : Collect light from broadband lamp with furnace operation, combustion gases and water, no subtraction.
7 : Collect light from broadband lamp with furnace operation, combustion gases, water, and candidate marker material. Spectra obtained during step 5 subtracted.

These steps are required to evaluate contributions to the spectrum from a variety of interferences. Comparing the spectra obtained in these steps indicates interfering lines.

Each of the above described reference spectra will have, besides the features attributable to specific experimental conditions, features of the light propagation in the room atmosphere. Absorption by water and carbon dioxide in the atmosphere is possible, but will be low, as the result of the short path length in the room air (approximately 70 cm in open air and another 50 cm inside the monochrometer).

Most features attributable to the carrier gas start showing up at elevated temperatures, when more molecular energy levels are populated and more transition lines can be reached. For the carrier gas used in most experiments, the carbon dioxide and water lines in the infrared have been clearly documented and can be found in most reference books.[16] The comparison of the spectra of the carrier gas at elevated temperatures with and without the potential marker species present will provide the contribution of the marker species.

Results

A summary overview of all the tests done, by material and wavelength, is given in Table IV. Results from these tests are described in this section. For each test, the species inserted into the furnace and the optical detection range are indicated.

**Pt, UV/Vis:** The literature survey summarized in Table III showed, that the dominant platinum emissions were located at wavelengths of 265.94 and 306.47 nm. However, no emission or absorption was detected at these wavelengths over the full temperature range from 800 to 1200 C. The cause is believed to be the low equilibrium vapor pressure of platinum metal ($10^{-18}$ – $10^{-12}$ bar). In combination with the relatively short absorption path of the furnace, the sensitivity is expected to be extremely low, and detection difficult.

In a related note it should be mentioned that while scanning platinum over the full range from 200 to 1500 nm, several absorption lines were discovered. Because the inclusion of the whole range in a figure would obscure the relevant details, only the parts of the observed spectrum that have noticeable features are shown. One doublet is located at 589 and 589.5 nm (Figure 7a), one at 766.4 and 769.9 nm (Figure 7b), and a series of lines runs from 920 to 960 nm (Figure 7c). Some features are slightly shifted from their literature values (Table III) due to instrument inaccuracies. The doublets correspond with sodium and potassium absorption, and the line series with water absorption. The strongest pair was the sodium doublet at 589 and 589.5 nm. Chemical analysis of the platinum used in the experiments verified the presence of substantial amounts of Na (300 ppm) and K (1500 ppm). The results are shown in Table V.

The potassium absorption is strongly dependent on the temperature as shown in Figure 8. At 1117 °C, small absorption lines appear at 766.4 nm and 769.9 nm. At 1149 °C, the absorption is substantial, and increases until the highest experimental temperature at 1210 °C. The increase in line strength is believed to be caused by an increase in the molecular population of the lower state of the transition during increase in temperature.

Another phenomenon is observed when the high temperature gas simulation is replaced with high temperature argon: the potassium absorption line intensity jumps by an order of magnitude. This jump is attributed to the increased stability of the potassium gas species under these conditions. Increasing the temperature from 1200 °C to 1400 °C shows a line reversal from absorption to emission, as the result of a larger molecular population of the species residing in the upper state of the transition due to the thermal energy absorption. This reversal is shown in Figures 9a though 9g. An interesting aspect of this reversal is that the emission is slightly shifted upwards from the absorption. No explanation for this shift has been found. Much of the noise in the spectra are caused by an interference by the furnace, and are furnace temperature dependent.

**Pt, IR:** From Figure 4a it can be seen that the theoretical vapor pressure of platinum dioxide in an equilibrium state with the simulated combustion gas at temperatures of 1200 °C is five to six orders of magnitude higher than that of the elemental species or the monoxide. Absorption or emission transitions, detectable with easily available equipment, and corresponding to vibrational levels of platinum dioxide, are located in the infrared region. The O-O stretch is located at 10.787 μm, the Pt-O bend at 14.286 μm and the Pt-O stretch at 24.096 μm. The latter absorption is not within the experimental capability, because the only window material transparent for light near 25 μm is extremely hygroscopic and difficult to utilize at high temperatures. Only the frequencies at 10.787 and 14.286 μm can be evaluated, as well as some of their combination frequencies. Combination frequencies are the result of multiple energy jumps accomplished within a single transition, yielding a larger energy jump and thus a lower wavelength of absorption or emission. Both single jump transitions and multiple jump transitions are governed by selection rules. For a theoretical explanation of transition rules, see Herzberg.[17]

The full range of interest from 2 to 18 micron, following the procedure outlined in the experimental section, was scanned. Results of the mid-IR scans (2000 – 10000 nm) are shown in Figure 10. Three sets of data are represented: an absorption scan with air at ambient conditions (solid lines); a scan with simulated exhaust gas (no water, ~10% $CO_2$) at 1200 °C (dashed lines); and a scan with platinum powder inside the furnace containing simulated exhaust gas (minus water) at 1200 °C (dotted lines). All spectra were obtained several times and proved to be repeatable. For each condition in Figure 10, two traces are shown. Small variations in the intensities can be seen throughout the spectra. This difference, however, is believed to be caused by small differences in experimental conditions, such as small alignment variations of the optics, differences in atmospheric conditions, and differences in temperatures. All three sets of spectra show the same features.

A comparison of the obtained absorption spectra, as shown in Figs. 10a, b and c, with the literature spectra of water and carbon dioxide[18] helps to identify features. The lack of intensity below ~2750 nm is believed to be a combination of $CO_2$ absorption as well as the low sensitivity of the MERCADTEL detector in this region. After approximately 2800 nm, the intensity increases rapidly and reaches a plateau at about 3000 nm. This constant intensity is sustained until a sudden drop occurs between 4200 and 4400 nm, which is believed to be caused by $CO_2$ only.

A series of absorption features between 5000 and 7500 nm occurs in all three cases. No clear indication about their origin is obvious, although atmospheric water vapor (~ 3%) could be a cause. A detail of the spectrum between 5000 and 7600, shown in Figure 10 b, clearly reveals that even though the intensity might vary slightly between cases, the basic features are present in all three cases, and can therefore not be attributed to the presence of platinum. After about 7500 nm, the signal decreases in intensity, as a result of a decreasing throughput of the monochromator. The mid-IR grating installed in the monochromator is optimized for 5000 nm, and is therefore expected to have maximum throughput at that wavelength. In the range upwards of 7500 nm, no features are detected.

One detail, however, stands out. The strong dip in the spectra at around 4300 nm displays non-negligible differences between the sets of spectra shown in Figure 10a. For ambient air, the absorption is relatively narrow. Including 10% $CO_2$ (combustion gas) at 1200 °C substantially widens the absorption feature, believed to be caused by the fact that at high temperature, many more energy levels are populated, thus many more transitions occur over a wider range of energy gaps. But the surprise shows up when platinum in inserted at the elevated temperatures. The absorption line bandwidth again jumps to a much wider profile, with a cause that can only be

speculated about, but seems to be related to the presence of a different species. Whether this phenomenon is particular for platinum, or also occurs with other species present is not known.

Subsequent tests were performed to verify whether platinum dioxide itself causes the line broadening. To that end, two tests were performed with platinum powder in a 1200 °C environment, one in pure argon, and one in pure oxygen. The argon was intended to eliminate the formation of platinum dioxide and to limit the platinum to elemental species. The oxygen was intended to increase the amount of platinum dioxide present in the flow. Results of these tests are shown in Figure 10c. Both the pure argon, and the pure oxygen measurements show the $CO_2$ absorption line, identical to the absorption line width in pure air. This absorption is believed to be taking place outside the furnace in the optical path between the source and the furnace, and between the furnace and the detector. Because the atmosphere outside the furnace is at room temperature, the temperature in the furnace will not play a role on the absorption line width, as can be seen from Figure 10c. From the four measurements shown in Figure 10c, only the absorption line with the combustion gas mixture at 1200 °C in the furnace shows a substantial $CO_2$ line broadening, due to the elevated temperature of the gas. As a result of these measurements, and the previous observation that the line broadening is increased with the presence of $PtO_2$ in the combustion gas mixture, it is becoming clear that this presence of $PtO_2$ in the gas phase has an effect on the line width of $CO_2$. Further investigation is needed to quantify this effect, and to verify whether this is isolated to $PtO_2$ only, or whether other species have the same effect. The platinum dioxide therefore does not show absorption under these conditions, but will affect the carbon dioxide absorption at elevated temperatures to broaden the absorption.

Results from tests in the upper range of the mid-IR (8000–18000 nm), with and without platinum inside the furnace, and in equilibrium with an argon-, oxygen-, or simulated exhaust gas environment, are shown in Figure 11. The peak at maximum intensity is located at 12000 nm, corresponding to the grating blaze wavelength. Spectral features at 10800 nm (carbon dioxide) and a series between 13500 and 15000 (unknown origin) are common between the various test parameter sets. Although the overall intensity varies between the different tests, no distinct spectral features were discovered which were different between the different conditions, pure exhaust gas, exhaust gas with platinum, platinum with argon, platinum with pure oxygen, and pure oxygen. These results were believed to indicate that platinum dioxide and/or platinum hydroxide do not absorb or emit within this wavelength range, and thus would not be a suitable candidate for marker material with the detection scheme used.

**CuO, UV/Vis:** The literature survey summarized in Table III showed that for arc excitation, copper transitions occurs at 324.8 and 327.4 nm. Copper oxide (CuO) is placed in the furnace and the temperature is slowly increased from 800 °C, while scanning the full range of wavelengths from 250 to 1500 nm. During this increase in temperature, a change from solid copper oxide to solid copper dioxide takes place, which melts at approximately 1244 °C.

$$2CuO_{(s)} \xrightarrow{1025\ ^{\circ}C} Cu_2O_{(s)} + \tfrac{1}{2} O_2 \xrightarrow{1244\ ^{\circ}C} Cu_2O_{(l)} \qquad (2)$$

The subscript (s) stands for solid and (l) for liquid. Copper vapor is in equilibrium with solid CuO, and solid and liquid $Cu_2O$ over the whole temperature range. At around 1157 °C, a weak absorption line starts appearing at 324.8 nm, followed by the appearance of the 327.4 nm absorption line at 1160 °C. With increasing temperature these absorption features intensify, with maximum absorption at the termination of the test at 1350 °C. The measured absorption as a function of wavelength is displayed in Figure 12. The measured intensity level shows a drift,

which varies with temperature and can be attributed to furnace interference to the detector. The two absorption peaks are clearly defined.

Figure 4b indicates that the equilibrium concentration of copper in the gas phase is of the order of $10^{-6}$ atm at 1200 °C, slightly higher than the $10^{-7}$ atm concentration of copper hydroxide and higher than the $10^{-8}$ atm concentration of copper oxide in the gas phase. In combination with the strong transition probability, this leads to the strong absorption features observed.

Observation of the remaining parts of the obtained spectra, not shown in Figure 12, do not lead to additional spectral features in the temperature range under consideration. Neither copper hydroxide around 535 nm, nor copper oxide around 606 nm can be detected at the concentrations available in the equilibrium gas phase.

Thermochemical calculations show that a number of copper species need to be considered, including copper hydroxide and copper oxide. Figure 3b shows that the concentration of $Cu_2$ is just too low for consideration. However, after careful review of the UV/Visible copper data, and the knowledge that copper oxide melts at a temperature too low to be of interest for the application being evaluated, no effort to obtain mid-IR spectra of copper oxide was made.

**ZnO, UV/Vis:** Zinc Oxide (ZnO) was placed inside the furnace and the spectrum was observed from 250 nm to 1500 nm over a temperature range from 800 to 1350 °C. As with copper oxide, zinc oxide placed in the furnace gives rise to both zinc oxide vapor and zinc vapor. Due to the low zinc oxide line strength (Table III), no zinc oxide spectral features were discovered, not even at the wavelength of highest transition probability, at 567.89 nm. Evaluating the equilibrium pressure of zinc vapor (between $10^{-10}$ and $10^{-6}$ atm in the range from 1000 to 1350 °C, see Fig. 4c), coupled with the low transition probability (relative to and indicated by the arc excitation linestrength of Table III), this result is understandable. At the highest temperatures evaluated, the zinc concentration equals the copper concentration, but the transition probability of copper is several orders of magnitude higher.

Over the infrared range from 2000 to 18000 nm, spectra are obtained with zinc oxide in the furnace at temperatures of 1200 °C. Equilibrium thermochemical calculations shown in Fig. 4c indicate that only the zinc monoxide needs to be considered. No features other than the water and carbon dioxide absorption are detected. The cause of absence of any zinc oxide absorption is believed to be the low concentration and the short path length at which the gas is at high temperature. Because the obtained spectra from ZnO are no different from the reference spectra in Figs. 10 and 11, they are not shown.

**Cr, UV/Vis:** Chromium is used as an indicator of the temperature sensitivity and overall experimental setup sensitivity. Chromium emission was detected in two combustion environments where stainless steel was placed inside hydrogen/oxygen flames at different pressures and fuel/air ratios. Chromium exhibits strong emission at 425.4, 427.4, and 428.9 nm, as shown in Figure 2a. However, spectral measurements in this region did not indicate the presence of chromium in a detectable amount up to 1400 °C, and the obtained spectra are not shown. This is most likely due to the low partial pressure of chromium in the oxidizing environment of this study. Figure 4d shows that the vapor pressure of chromium metal is from 5 to 8 orders of magnitude lower than the vapor pressures of its oxides and hydroxides under the experimental conditions of the tests.

Summary and Conclusions

The potential for using selected species as marker material for in-flight detection of TBC coating spalling has been evaluated in a laboratory environment. Thermochemical equilibrium software was used to screen a large number of potential marker materials. Only species with known thermochemical data were evaluated. An additional consideration was the potential spectroscopic absorption/emission strength. Four potential marker materials were selected, platinum, copper, indium, and zinc. Indium was rejected due to the low melting temperature.

The three remaining species were heated in a simulated exhaust gas environment at a range of temperatures (inside a high temperature furnace). Species emission and absorption characteristics were determined over a spectral range from 250 to 18000 nm, with a small hiatus from 1500 to 2000 nm due to equipment shortcomings. Different monitoring techniques were employed in the area of UV/Visible/near-IR and the mid-IR region due to the varying component transmittance and quantum sensitivities.

Platinum did not show emission or absorption spectra, either from the elemental vapor, or from the oxide or hydroxide vapors. One feature was detected. The carbon dioxide absorption line near 4300 nm, narrow in atmospheric conditions, substantially broadened due to the high temperature carbon dioxide gas inside the furnace. Additional broadening occurred in the presence of platinum vapor species. Additional tests showed that this was not a contribution from the platinum vapor species, but more a broadening caused by interference between carbon dioxide and platinum vapor species. Whether this interference is unique for platinum vapor species, or will also occur with other collision partners has not been determined, but could be the key and deserves further investigation.

Additionally, platinum powder inserted inside the furnace at high temperature caused strong absorption lines to appear around 589 and 768 nm. Chemical identification showed that these lines were caused by sodium and potassium impurities in the platinum powder. The potassium lines showed reversal from absorption to emission with increasing temperature, a phenomenon which is associated with increased population densities of higher energetic levels of the species at increasing temperatures. Because potassium and sodium are common contaminants throughout the engine, they are not good candidates for specific marker materials. Other elements in the same elemental groups, such as rubidium, might provide a mechanism for marker material. For the current study, rubidium has not been considered due to the absence of thermochemical data.

Copper vapor from copper oxide exhibits strong emission lines at elevated temperatures. Around 1160 °C, two lines appear at 325 and 327 nm, which grow rapidly in intensity with increasing temperature. Because of the temperature dependence, copper oxide would be an ideal marker material for TBC coating spalling. The results from the vapor from CuO evaluation showed that the absorption of copper jumps between 1160 and 1300 °C, just 140 °C. However, because the melting temperature of copper oxide ($Cu_2O$) is relatively low, it is deemed to be unsuitable for inclusion in the TBC bondcoat, and is therefore not considered further. IR absorption or emission spectroscopy of copper species was not tried.

Spectroscopic measurements of vapor from zinc oxide in the UV/Visible/near-IR range showed no detectable absorption. No lines are detected at the literature values of 330 and 334.5 nm for zinc vapor, possibly because of the low equilibrium vapor pressure coupled with the low transition probability. No mid-IR measurements of zinc oxide were performed. Based on the preliminary tests performed, zinc oxide does not appear to be a good marker candidate.

Chromium, a widely occurring material in engine environments was also evaluated. In the range of temperature values characterized, from 800–1200 °C, no absorption or emission lines were found. This contrasts with the emission found in both the SSME tests and the in-house hydrogen/oxygen rocket tests. The main difference between the current tests and the two combustion tests was the higher temperature range of the combustion tests (T~2800 K) and the different combustion gas composition (hydrogen/oxygen/water for the combustion tests).

References


1. G.C. Madzsar, R.L. Bickford, and D.B. Duncan, "An Overview of In-Flight Plume Diagnostics for Rocket Engines," AIAA–92–3785, 28th JPC Conference and Exhibit, July 6–8, 1992, Nashville, TN.

2. P.F. Paradis, "Spectroscopic Diagnostics of Aircraft Engines at NRC," AIAA–97–2661, 33rd JPC Conference and Exhibit, July 6–9, 1997, Seattle, WA.

3. Unpublished data obtained at Combustion Laboratories of NASA Glenn On-Board Propulsion Branch.

4. J.N. Forkey, W.R. Lempert, and R.B. Miles, "Corrected and Calibrated $I_2$ Absorption Model at Frequency Doubled Nd:YAG Laser Wavelengths," Applied Optics, Vol. 36, 1997, pp. 6729–6738.

5. M.W. Chase, Jr., C.A. Davies, J.R. Downey, Jr., D.J. Frurip, R.A. McDonald, and A.N. Syverud, Editors, JANAF Thermochemical Tables, 3rd ed., American Chemical Society and American Physical Society, New York (1985).

6. Alan Dinsdale, SGTE Data for Pure Elements, Calphad, Vol. 15, pp. 317–425, (1991).

7. L.V. Gurvich, V.S. Iorish, D.V. Chekhovskoi, and V.S. Yungman, IVTANTHERMO – A Thermodynamic Database and Software System for the Personal Computer, Begell House/NIST, 1993.

8. V.P. Glushko, L.V. Gurvich, G.A. Bergman, I.V. Veitz, V.A. Medvedev, G.A. Khachkuruzov and V.S. Jungman, Editors, Thermodynamics of Pure Substances, 3rd ed., Nauka Publishers (1978).

9. O.H. Krikorian, High Temperatures - High Pressures, 14, 387 (1982).

10. B.B. Ebbinghaus, Combustion and Flame, 93, 119 (1993).

11. A. Hashimoto, "The Effect of $H_2O$ Gas on Volatilities of Planet-Forming Major Elements: I. Experimental Determination of Thermodynamic Properties of Ca-, Al-, and Si-Hydroxide Gas Molecules and its Application to the Solar Nebula," Geochim. Cosmochim. Acta 56, 511–32 (1992).

12. G. Eriksson and K. Hack, ChemSage - A Computer Program for the Calculation of Complex Chemical Equilibria, Met. Trans. B, 21B, 1013 (1990).

13. R.W.B. Pearse and A.G. Gaydon, The Identification of Molecular Spectra 4th Ed., Chapman and Hall, London, p. 287.

14. W.R. Brode, Chemical Spectroscopy, 2nd Ed., Wiley and Sons, 1958.

15. WINSPEC v. 1.6.2.24– Princeton Instruments, Inc., 1997.

16. GRAMS v. 2.1 – Galactic Industries, Inc., 1998.

17. Herzberg, G., Molecular Spectra and Molecular Structure I. Spectra of Diatomic Molecules, 2nd Ed., Krieger Pub. Co., 1989 Reprint.

18. CRC Handbook of Chemistry and Physics, 80th ed., 1999, p. 14-24.

**Table I: Thermochemical screening of candidate marker materials.**

| Element | Thermochemical Data Source | Predominant Volatile Species |
|---|---|---|
| Li | SGTE | LiOH |
| Mg | SGTE | $Mg(OH)_2$ |
| Ca | SGTE | $Ca(OH)_2$ |
| Sr | SGTE | $Sr(OH)_2$ |
| Ba | SGTE | $Ba(OH)_2$ |
| Nb | SGTE + Krikorian | $NbO(OH)_3$ |
| Mo | SGTE | $MoO_2(OH)_2$ |
| W | SGTE | $WO_2(OH)_2$ |
| Mn | SGTE + IVTANTHERMO | $MnO_2$, MnO |
| Ru | SGTE + Krikorian | $RuO_3$ |
| Rh | SGTE + Krikorian | $RhO_2$ |
| Pt | SGTE | $PtO_2$ |
| Cu | SGTE + IVTANTHERMO | Cu |
| Zn | SGTE + IVTANTHERMO | Zn |
| B | SGTE | BO(OH) |
| Al | SGTE + Glushko | $Al(OH)_3$, $Al(OH)_2$ |
| Ga | SGTE + IVTANTHERMO | GaOH |
| In | SGTE + IVTANTHERMO | InOH |
| Tl | SGTE + IVTANTHERMO | TlOH |
| Si | SGTE + Krikorian + Hashimoto | $SiO(OH)_2$ |
| Ce | SGTE + Krikorian | $CeO(OH)_2$ |
| Eu | SGTE + Krikorian | EuO(OH) |
| Pr | SGTE + Krikorian | PrO(OH) |

**Table II: Melting points of relevant species.**

| | Melting Point (°C) | Notes |
|---|---|---|
| Pt | 1772 | |
| Zn | 419 | |
| ZnO | 1975 | |
| Cu | 1083 | |
| CuO | 1244 | Transforms to $Cu_2O$ at 1025 $^oC$ |
| In | 157 | |

**Table III: Pre-selected marker candidate spectral characteristics.**

| | Dissoc. Energy (kcal) | Transition Wavelength (nm) | Line Strength (arbitrary) | Remarks | Reference |
|---|---|---|---|---|---|
| Pt | | 265.94<br>283.03<br>299.80<br>306.47 | 2000<br>1000<br>1000<br>2000 | Arc discharge | 13 |
| PtO | | 544.56<br>566.30<br>590.23<br>621.06<br>654.85 | | In arcs and hollow cathode discharge. No intensities available. | 12 |
| $PtO_2$ | | | | No spectral data available | |
| $Pt_3(OH)_4$ | | | | No spectral data available | |
| Zn | | 330.29<br>334.50 | 700<br>800 | Arc discharge | 13 |
| $Zn_2$ | 6 | 213.9<br>305.0<br>307.6 | | Hollow cathode tube | 12 |
| ZnO | 65 | 343.58<br>532.69<br>536.94<br>558.12<br>567.89 | ?<br>8<br>8<br>7<br>10 | These are for arc excitation. It is not sure whether these lines are caused by ZnO or a polyatomic emitter | 12 |
| $Zn(OH)_2$ | | | | No spectral data available | |
| Cu | | 324.75<br>327.40 | 5000<br>3000 | Arc discharge | 13 |
| $Cu_2$ | 46 | 490.15<br>491.90 | 8<br>10 | Emission and absorption in a King furnace | 12 |
| CuO | 66 | 418.2<br>445.3<br>445.7<br>604.50<br>605.93<br>616.16 | Weak<br>8<br>8<br>8<br>10<br>9 | Detected in copper arcs or flames with copper salts. | 12 |
| Cu(OH) | 61 | 535.0-555.0<br>615.0-625.0<br>524.6<br>532.4<br>535.6<br>537.1<br>537.46<br>538.8<br>541.86<br>543.4<br>545.7 | Strong band<br>Weak band | Occurs in flames. Green flame color due to formation. Some bands occur in green (510 – 560 nm) | 12 |

**Table IV: Wavelength range and materials tested.**

| Materials Inserted in Furnace | UV/Vis./near-IR | Mid-IR Low Range | Mid-IR High Range |
|---|---|---|---|
| Pt | d | d | d |
| Pt/Na | d | d | d |
| Pt/K | d | d | d |
| CuO | d | nd | nd |
| ZnO | d | d | nd |
| CrO | d | nd | nd |

**Definition: nd = not done; d = done.**

**Table V: Chemical analysis of platinum powder used in spectroscopic evaluation.**

| Test | Rslt | Units | Rpts | StdDev | Comnt1 |
|---|---|---|---|---|---|
| CA | 70 | ppm | 3 | 3.283 | |
| CU | 15 | ppm | 3 | 0.751 | |
| FE | 50 | ppm | 3 | 10.553 | |
| K | 1500 | ppm | 3 | 12.492 | |
| MN | 5 | ppm | 3 | 0.746 | |
| NA | 300 | ppm | 3 | 10.972 | |
| PD | | | | | Not Detecte |
| RB | | | | | Not Detecte |
| SI | 120 | ppm | 3 | 2.489 | |
| TI | 30 | ppm | 3 | 1.79 | |
| ZN | 22 | ppm | 3 | 0.887 | |
| ZR | | | | | Not Detecte |

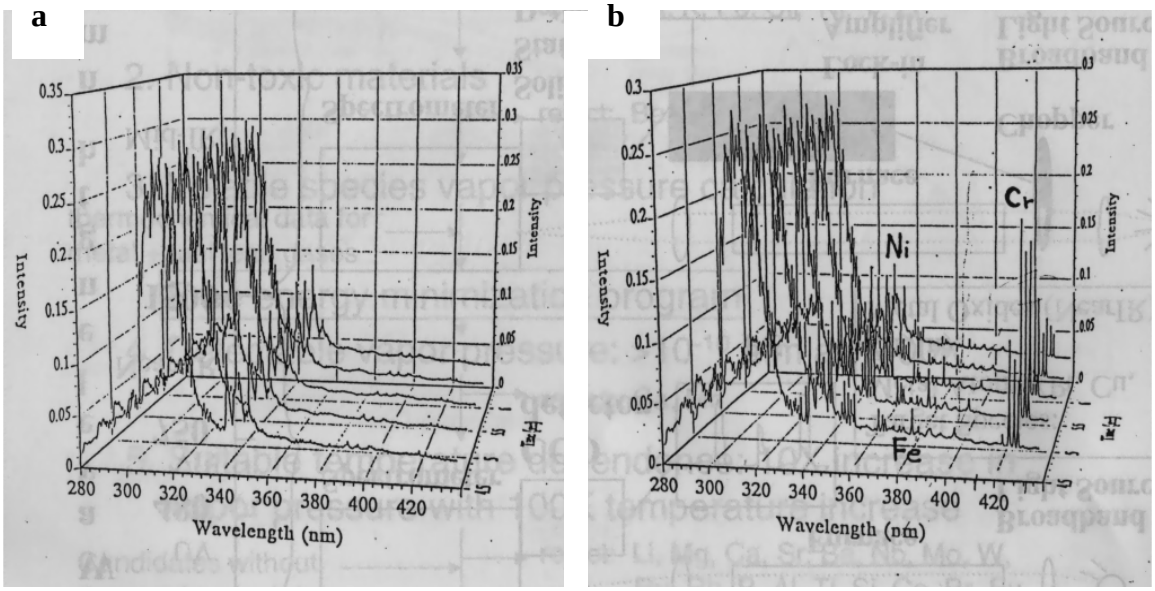


**Figure 1: Examples of plume metals emission during SSME test firings. a) normal operation with OH-emission and background chemiluminescence, b) erosive failure during operation with metallic species emission clearly visible.**

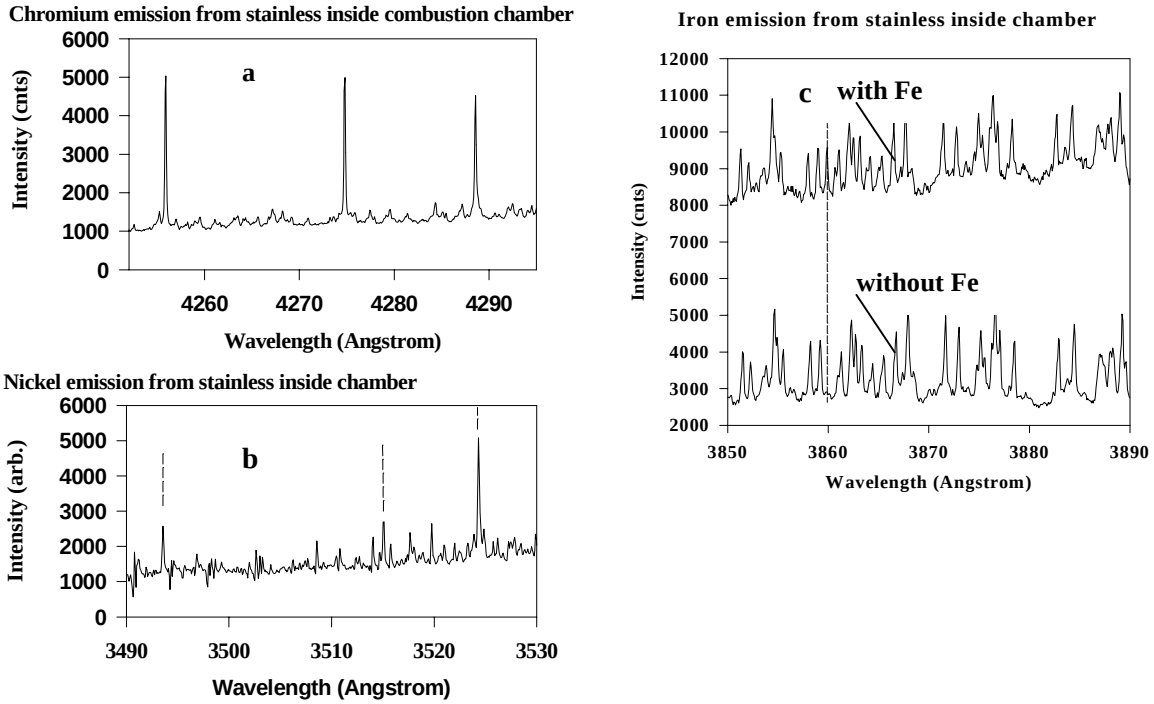


**Figure 2: Emission of stainless inside high temperature flame. a) Chromium, b) Nickel, c) Iron.**

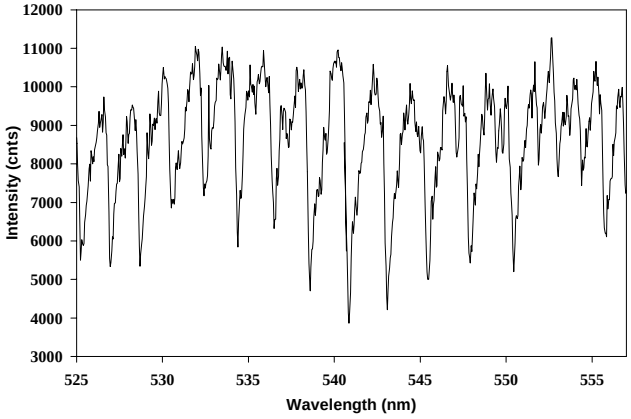


**Figure 3: Absorption of iodine ($I_2$) vapor in heated cell.**

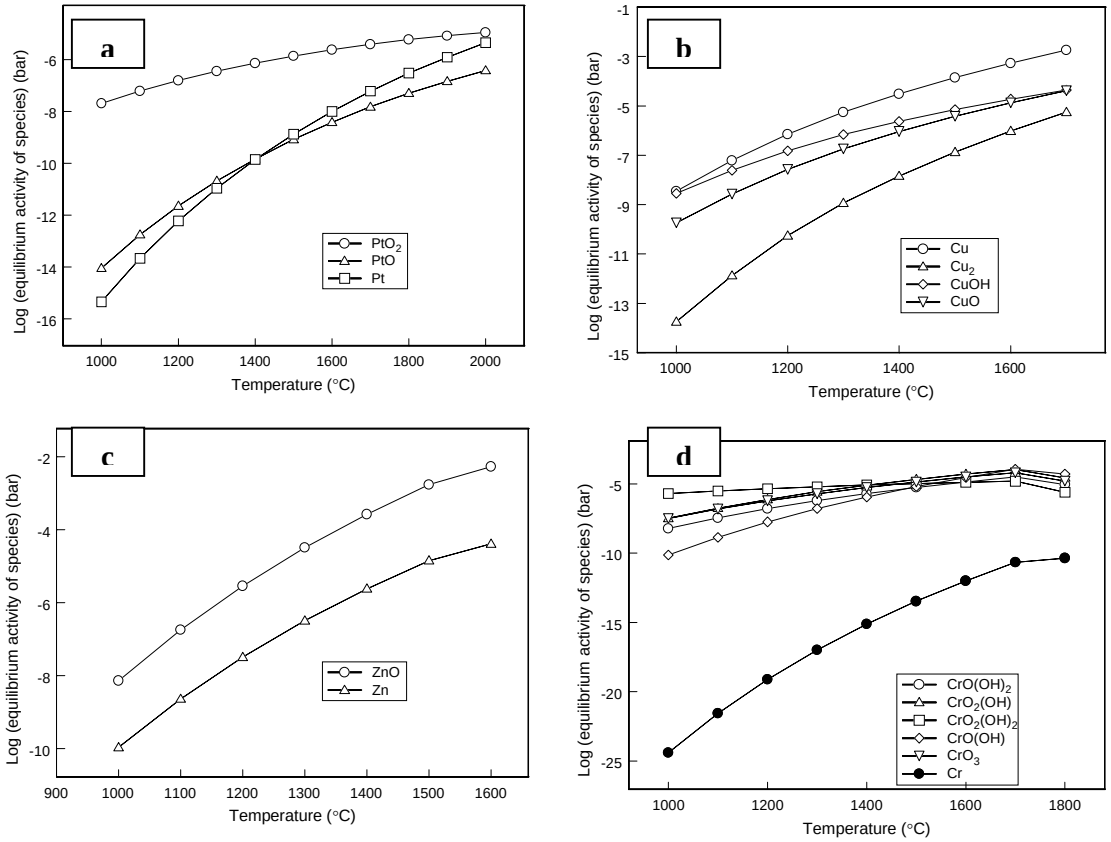


**Figure 4: The vapor pressure of volatile species of Cu, Zn, Pt, and Cr as a function of temperature.**

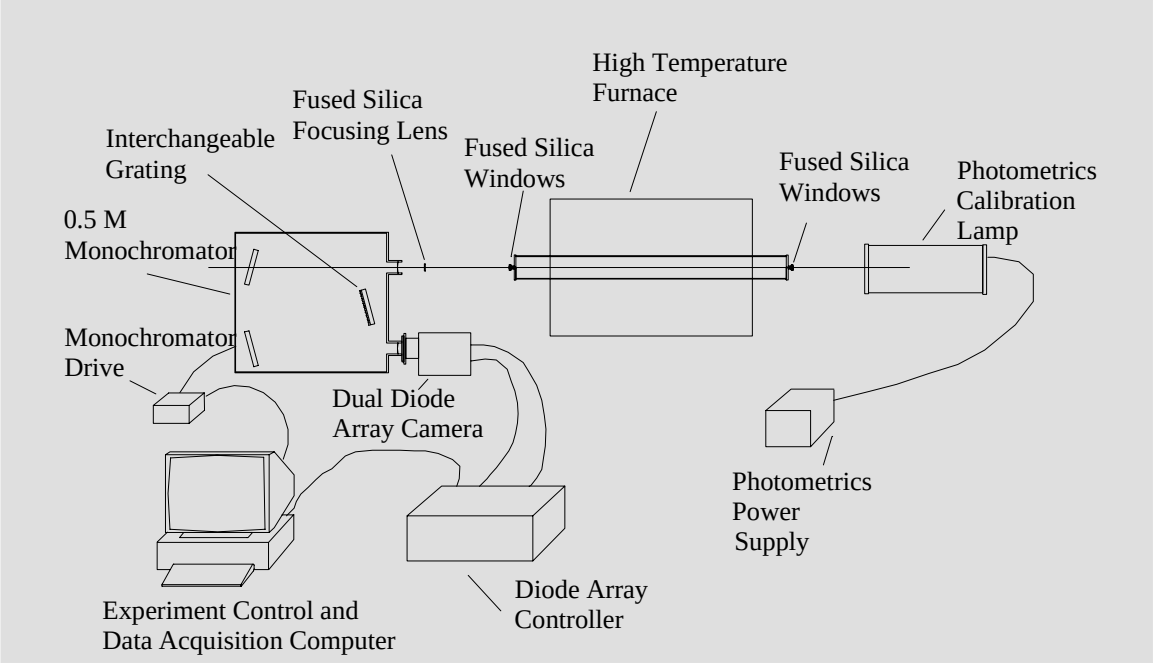


**Figure 5: Detection scheme for ultraviolet and visible detection from 250 – 1500 nm.**

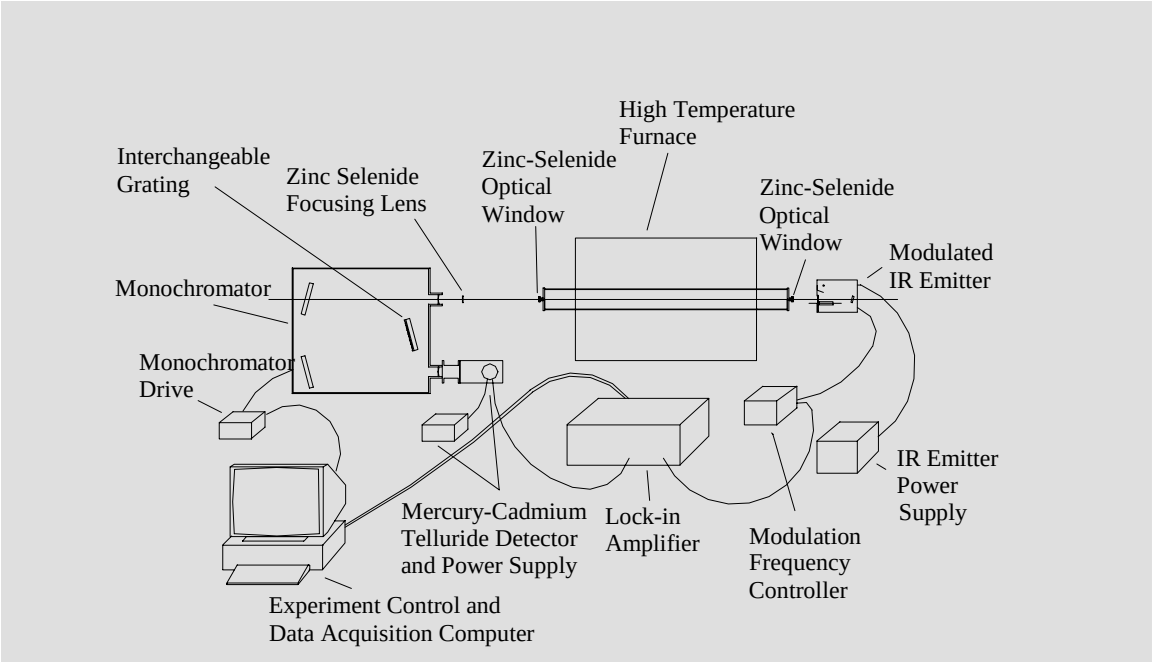


**Figure 6: Detection scheme for infrared detection from 2000 – 18000 nm.**

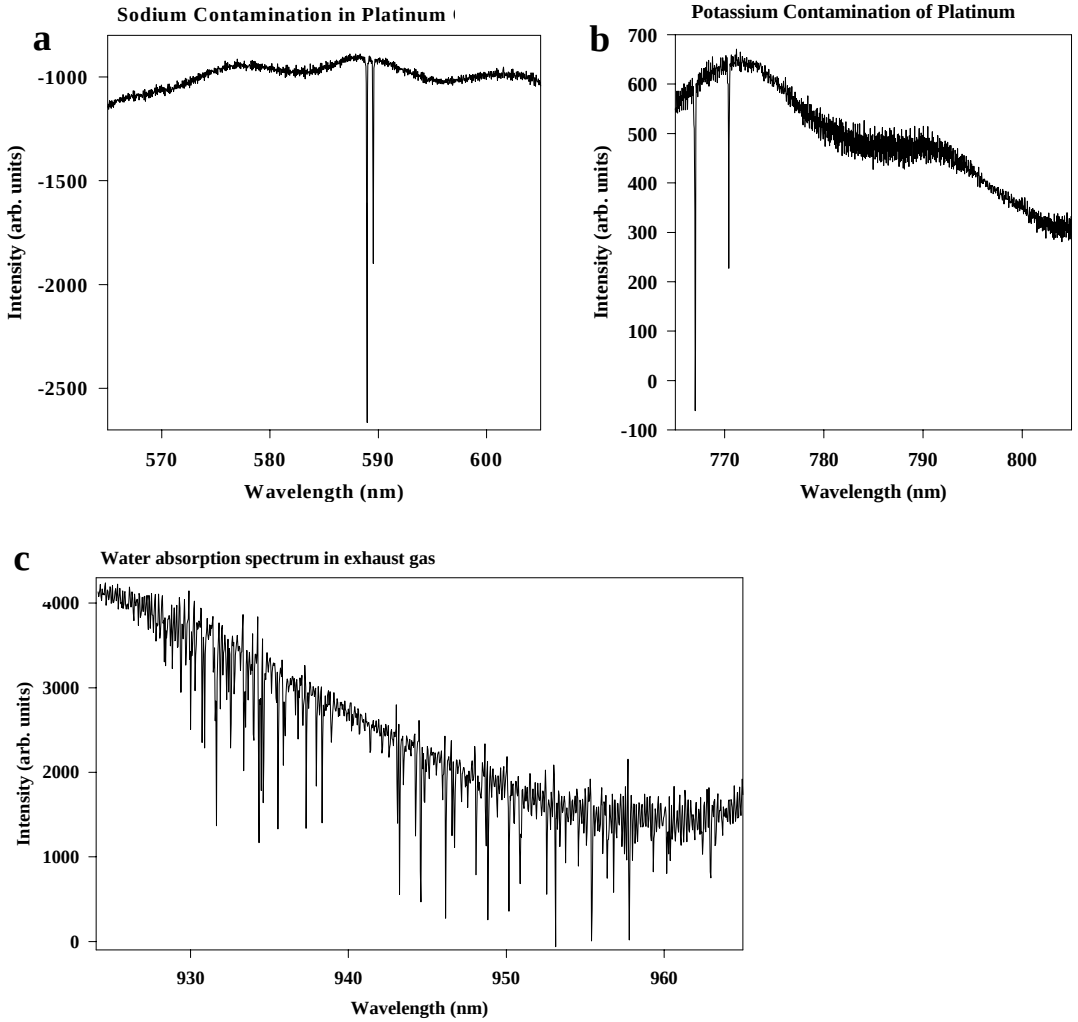


**Figure 7: Observed absorption lines caused by: a) sodium contamination of platinum, b) potassium contamination of platinum, c) water in the simulated exhaust gas.**

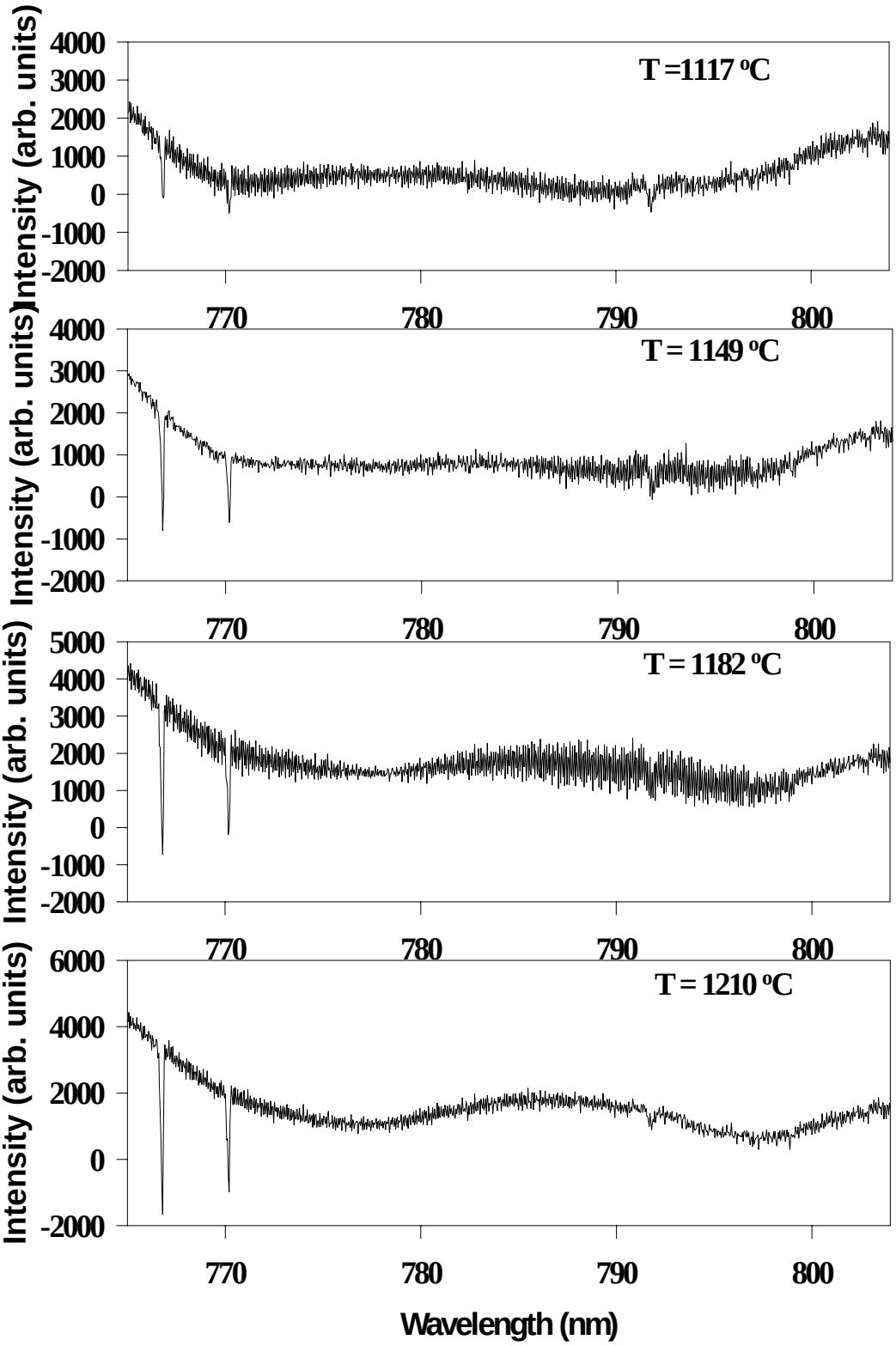


**Figure 8: Potassium impurity absorption in platinum as a function of temperature in combustion gas mixture.**

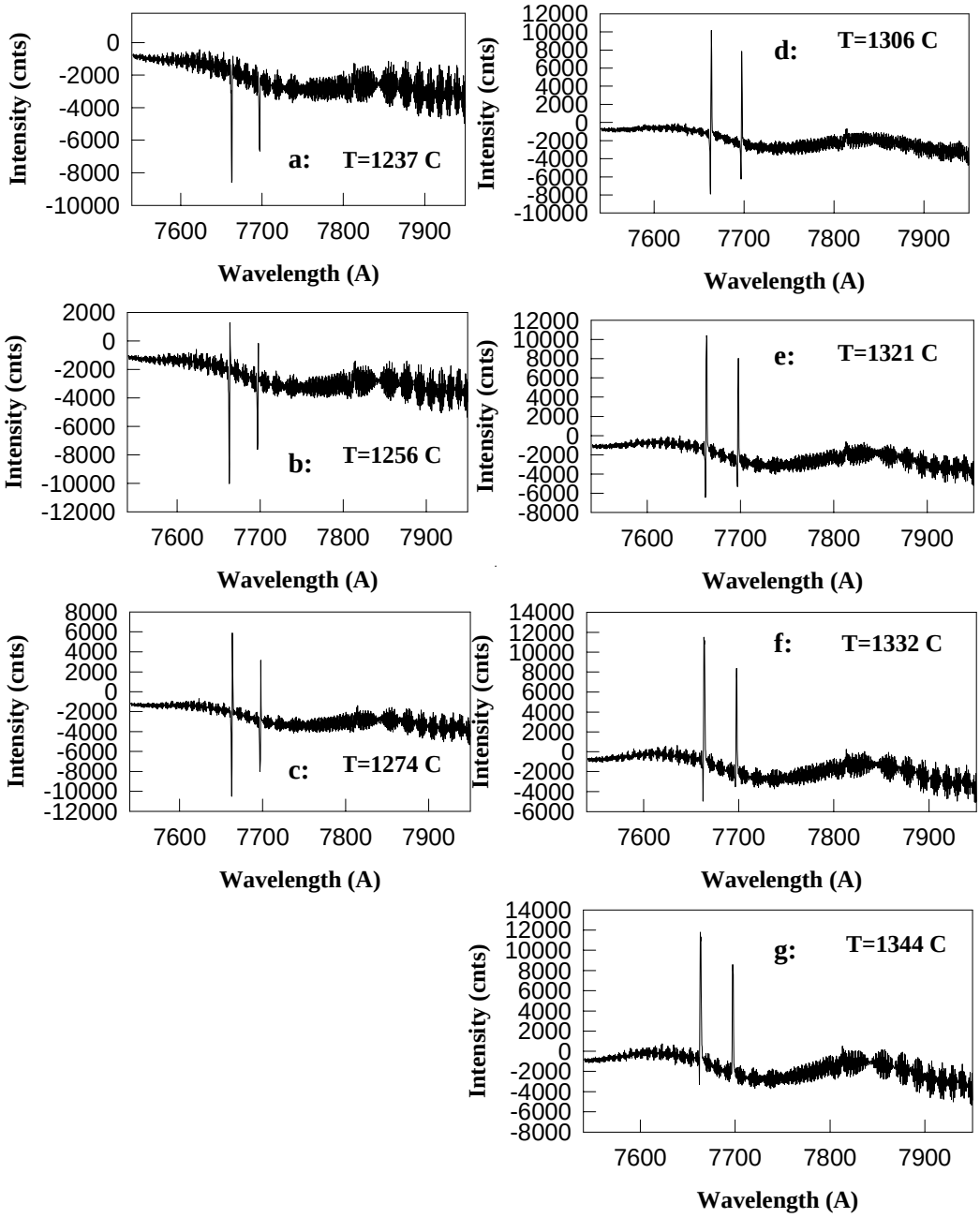


**Figure 9: Absorption/emission reversal as a function of temperature for potassium impurities in platinum in an argon atmosphere.**

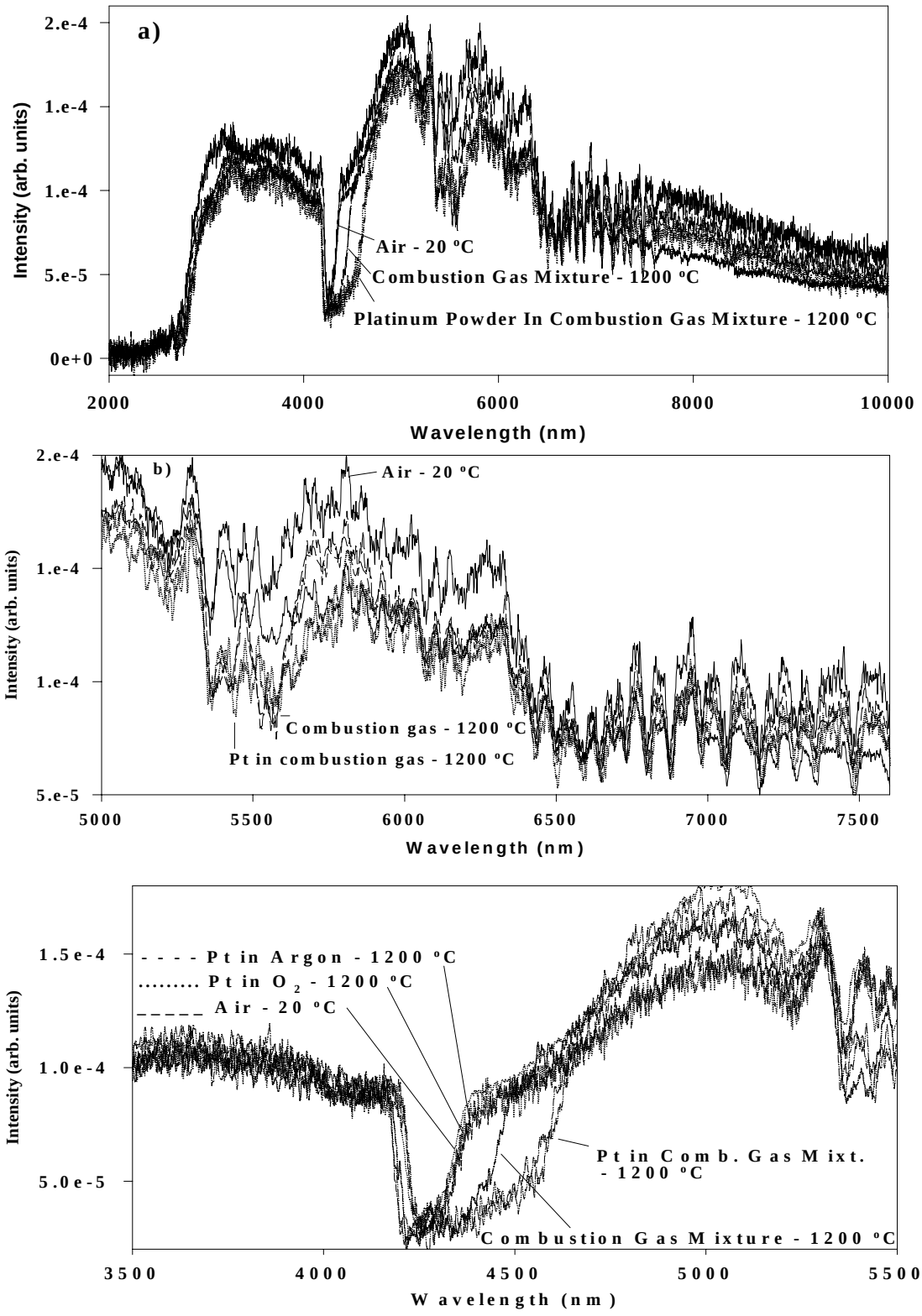


**Figure 10: Platinum dioxide effect on mid-IR spectrum of simulated exhaust gas. a) full spectrum, b) detail of section between 5000 and 7600 nm, c) detail of absorption line near 4300 nm.**

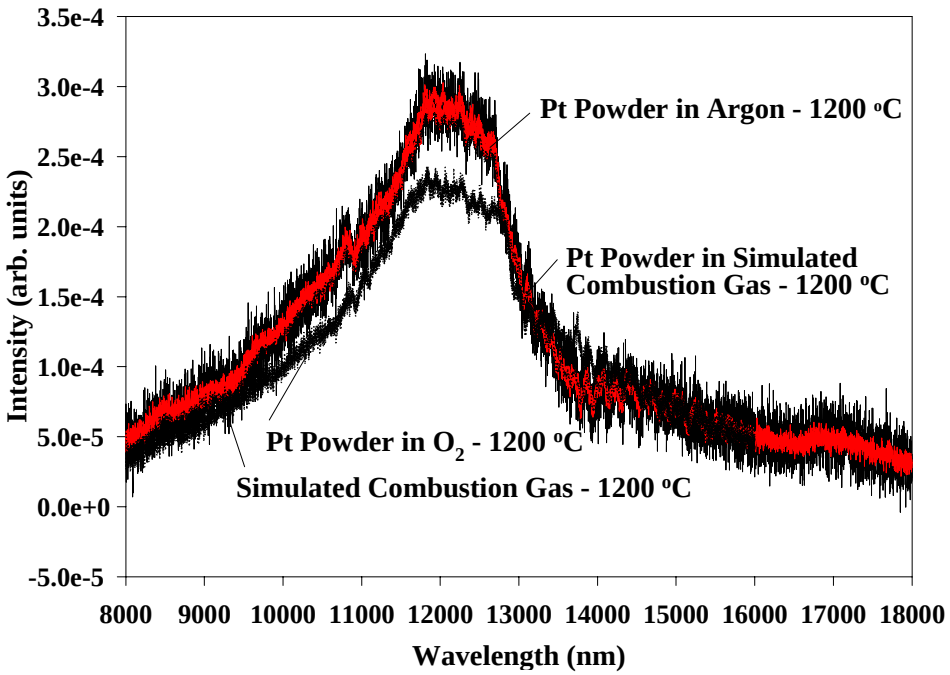


**Figure 11: Comparison of the upper range of the mid-IR spectrum of simulated exhaust gas with and without platinum powder inside furnace at 1200 °C.**

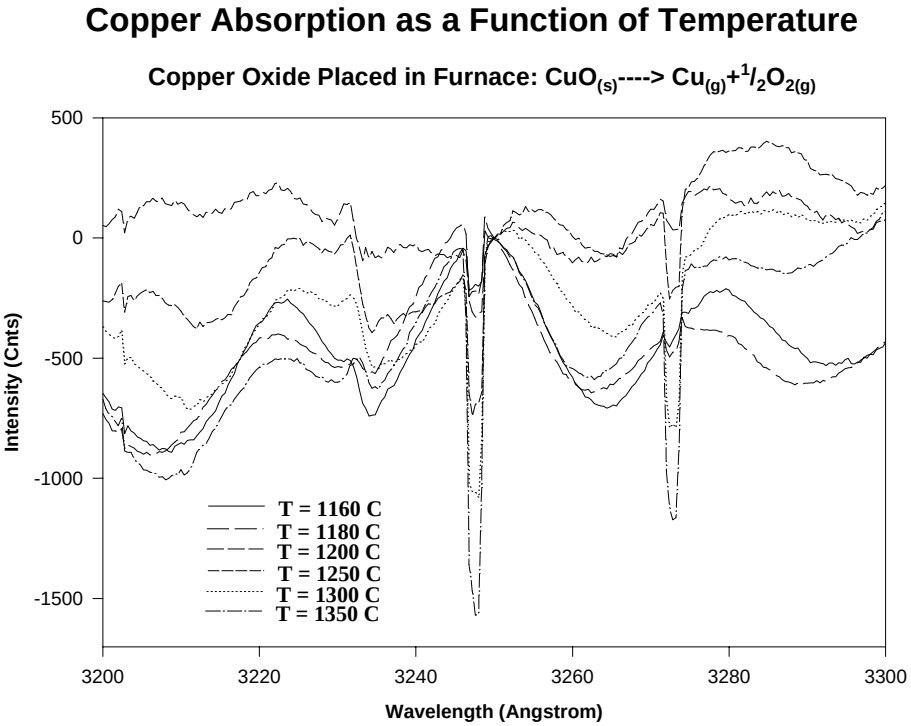


**Figure 12: Absorption of copper vapor as a function of temperature.**

# REPORT DOCUMENTATION PAGE

*Form Approved*
*OMB No. 0704-0188*



| 1. AGENCY USE ONLY (*Leave blank*) | 2. REPORT DATE | 3. REPORT TYPE AND DATES COVERED |
|---|---|---|
| | January 2001 | Final Contractor Report |

**4. TITLE AND SUBTITLE**

Investigation Into Spectroscopic Techniques for Thermal Barrier Coating Spall Detection

**5. FUNDING NUMBERS**

WU–274–00–00–00
NAS3–98008

**6. AUTHOR(S)**

Wim de Groot and Beth Opila

**7. PERFORMING ORGANIZATION NAME(S) AND ADDRESS(ES)**

Dynacs Engineering Company, Inc.
2001 Aerospace Parkway
Brook Park, Ohio 44142

**8. PERFORMING ORGANIZATION REPORT NUMBER**

E–12465

**9. SPONSORING/MONITORING AGENCY NAME(S) AND ADDRESS(ES)**

National Aeronautics and Space Administration
Washington, DC 20546–0001

**10. SPONSORING/MONITORING AGENCY REPORT NUMBER**

NASA CR—2001-210468

**11. SUPPLEMENTARY NOTES**

Wim de Groot, Dynacs Engineering Company, Inc., 2001 Aerospace Parkway, Brook Park, Ohio 44142, and Beth Opila, Cleveland State University, 1983 E. 24th Street, Cleveland, Ohio 44115–2403. Project Manager, Jim Gaunter, Turbomachinery and Propulsion Systems Division, NASA Glenn Research Center, organization code 5880, 216–977–7435.

**12a. DISTRIBUTION/AVAILABILITY STATEMENT**

Unclassified - Unlimited
Subject Category: 07 Distribution: Nonstandard

This publication is available from the NASA Center for AeroSpace Information, 301–621–0390.

**12b. DISTRIBUTION CODE**

**13. ABSTRACT** ***(Maximum 200 words)***

Spectroscopic methods are proposed for detection of thermal barrier coating (TBC) spallation from engine hot zone components. These methods include absorption and emission of airborne marker species originally embedded in the TBC bond coat. In this study, candidate marker materials for this application were evaluated. Thermochemical analysis of candidate marker materials, combined with additional constraints such as toxicity and uniqueness to engine environment, provided a short list of four potential species: platinum, copper oxide, zinc oxide, and indium. The melting point of indium was considered to be too low for serious consideration. The other three candidate marker materials, platinum, copper oxide, and zinc oxide, were placed in a high temperature furnace, and emission and absorption properties were measured over a temperature range from 800–1400 °C and a spectral range from 250 to 18000 nm. Platinum did not provide the desired response, likely due to the low vapor pressure of the metallic species and the low absorption of the oxide species. It was also found, however, that platinum caused a broadening of the carbon dioxide absorption at 4300 nm. The nature of this effect is not known. Absorption and emission caused by sodium and potassium impurities in the platinum were found in the platinum tests. Zinc oxide did not provide the desired response, again, most likely due to the low vapor pressure of the metallic species and the low absorption of the oxide species. Copper oxide generated two strongly temperature dependent absorption peaks at 324.8 and 327.4 nm. The melting point of copper oxide was determined to be too low for serious consideration as marker material.

| 14. SUBJECT TERMS | 15. NUMBER OF PAGES |
|---|---|
| Spectroscopy; Thermal barrier coating; Spalling | 30 |
| | 16. PRICE CODE: A03 |

| 17. SECURITY CLASSIFICATION OF REPORT | 18. SECURITY CLASSIFICATION OF THIS PAGE | 19. SECURITY CLASSIFICATION OF ABSTRACT | 20. LIMITATION OF ABSTRACT |
|---|---|---|---|
| Unclassified | Unclassified | Unclassified | |